coatings

*Article*

# Self-Healing UV-Curable Urethane (Meth)acrylates with Various Soft Segment Chemistry

**Paulina Bednarczyk [1,*], Paula Ossowicz-Rupniewska [1], Joanna Klebeko [1], Joanna Rokicka [1], Yongping Bai [2,3] and Zbigniew Czech [1]**

[1] Department of Chemical Organic Technology and Polymeric Materials, Faculty of Chemical Technology and Engineering, West Pomeranian University of Technology in Szczecin, Piastów Ave. 42, 71-065 Szczecin, Poland; possowicz@zut.edu.pl (P.O.-R.); joanna.klebeko@zut.edu.pl (J.K.); psa_czech@wp.pl (Z.C.)
[2] School of Chemistry and Chemical Engineering, Harbin Institute of Technology, Harbin 150001, China
[3] Wuxi HIT New Material Research Institute Co., Ltd., Wuxi 214000, China
* Correspondence: bednarczyk.pb@gmail.com or paulina.bednarczyk@zut.edu.pl

**Abstract:** This study explores the synthesis and evaluation of UV-curable urethane (meth)acrylates (UA) incorporating a Diels–Alder adduct (HODA), diisocyanate, poly(ethylene glycol), and hydroxy (meth)acrylate. Six UAs, distinguished by the soft segment of polymer chains, underwent comprehensive characterization using FTIR and NMR spectroscopy. Real-time monitoring of the UV-curing process and analysis of self-healing properties were performed. The research investigates the influence of various molecular weights of PEGs on the self-healing process, revealing dependencies on photopolymerization kinetics, microstructure, thermal properties, and thermoreversibility of urethane (meth)acrylates. This work provides valuable insights into the development of UV-curable coatings with tailored properties for potential applications in advanced materials.

**Keywords:** photocuring; urethane acrylate oligomers; self-healing polymers; Diels–Alder reaction photopolymerization; coatings



**Citation:** Bednarczyk, P.; Ossowicz-Rupniewska, P.; Klebeko, J.; Rokicka, J.; Bai, Y.; Czech, Z. Self-Healing UV-Curable Urethane (Meth)acrylates with Various Soft Segment Chemistry. *Coatings* **2023**, *13*, 2045. https://doi.org/10.3390/coatings13122045

Academic Editors: Andriy Voronov and Roman A. Surmenev

Received: 31 October 2023
Revised: 23 November 2023
Accepted: 1 December 2023
Published: 5 December 2023



## 1. Introduction

Self-healing coatings have garnered notable interest in recent years for their capacity to rectify damage and prolong the lifespan of diverse materials. One avenue for crafting self-healing coatings involves leveraging reversible covalent bonds, exemplified by the Diels–Alder reaction [1,2]. Recognized as a reversible reaction between a diene and a dienophile [3], the Diels–Alder reaction presents a viable strategy for introducing dynamic covalent bonds into coatings, enabling them to undergo repair processes when subjected to specific conditions, such as heat or mechanical stress. By incorporating these dynamic covalent bonds into a coating, the coating can self-heal when damaged [4]. When the surface is scratched or otherwise damaged, the dynamic covalent bonds within the coating can break and reform, effectively repairing the damage. This process can repeatedly occur, extending the service life of the coating and the underlying material [5,6]. One advantage of Diels–Alder-based self-healing coatings is that they can be designed to have specific properties, such as a particular rate of bond exchange or sensitivity to certain stimuli. This allows for the development of tailored coatings that can provide optimal performance in specific applications [7]. In summary, self-healing coatings based on the Diels–Alder reaction offer a promising approach to extending the service life of various materials by repairing damage via the use of dynamic covalent bonds [3,8,9].

Photopolymerization is the process of curing polymeric materials by irradiating them with light. Acrylates are a group of polymers that are often used in photopolymerization due to their reactivity and ability to cure quickly when exposed to UV irradiation [10,11]. Photopolymerization of acrylates is used in many fields, including the automotive industry,

medicine, printing, and the production of optical materials. It is a fast, easy-to-use, and controllable process, making it very popular in the industry [11–15]. Among the acrylates, urethane (meth)acrylates (UAs) can be distinguished. UV-curable oligomers, known as UAs, exhibit superior chemical and mechanical characteristics when employed in the formulation of UV-curable coatings. These coatings can offer either rigid or flexible properties, depending on factors such as molecular weight, functionality, and chemical structure [16]. Noteworthy advancements have been observed when implementing UAs in coatings for various applications, including metals, mobile phones, and electronic devices [15,17]. The synthesis of UAs involves the reaction between isocyanate and compounds featuring hydroxyl groups [18]. In the structure of the urethane (meth)acrylates carbon chain, there are mainly three components: (i) the (meth)acrylate group responsible for curing the resins, (ii) the "hard" segment, and (iii) the "soft" segment. The soft segments in urethane acrylate are thermoplastic elastomers in the form of, e.g., poly(ethylene glycol) (PEG) that are responsible for the flexibility and pliability of the material [19].

Poly(ethylene glycol)s, commonly abbreviated as PEGs, represent a significant category of polymeric materials in various applications [14]. The properties of PEG-based oligomers depended on the PEG molecular weight [20]. With the elevation of molecular weight, the morphological characteristics of PEG transitioned to liquid, viscous, and solid states [20]. PEG is a polyether compound with low surface tension that reacts easily with other chemicals. When PEG is added to elastomers, it creates strong bonds between them, which contributes to improving their mechanical and thermal properties [21]. PEG is also hydrophilic, meaning it attracts water and helps keep elastomers flexible even at low temperatures. These properties make PEG a popular addition to urethane acrylate soft segments, which contribute to improving their quality and performance in many applications, such as the coating industry, the production of polymeric products such as medical bands, protectors, insulation materials, and many more [22]. The scientific community has made substantial progress in exploring and innovating new applications for systems incorporating PEG. Notably, these materials have garnered significant interest, particularly in the coatings industry [5,13], the development of pressure-sensitive adhesives [23,24], hydrogels [25–27], and diverse drug delivery applications. This encompasses approaches such as direct PEGylation of therapeutics [28,29] and the utilization of PEG-based carriers [30], such as nanoparticles [31,32], dendrimers [5,15,33], or micelles [32,34,35]. Researchers are currently investigating the impact of PEG's molecular weight on polymer properties. In a study by Xiang et al., a comparative analysis was conducted on the performance of UV-curable flexible hyperbranched polyurethane acrylate (F-HBPUA), which incorporated flexible segments such as PEG200 and PEG600 [36]. In a distinct investigation, Ji et al. developed a photocuring ink featuring acryloyl-modified polyethylene glycol (AcrylPEG), generating test samples via 3D printing technology and evaluating the influence of varied molecular weights of PEG on sample performance [20]. Additionally, Feng et al. demonstrated that a slight increase in PEG content led to improvements in the tensile strength, ductility, and impact resistance of epoxy resin.

PEG has gained widespread recognition as a flexible monomer for enhancing the properties of photocurable materials [20]. Recent attention has focused on incorporating functional groups into PEG-related materials, including those responsible for polymer self-healing [37–42]. Typically, two approaches are employed for PEG functionalization, involving the modification of terminal hydroxyl groups via a sequence of reactions to yield derivatives containing diene or dienophile structures for employment in the Diels–Alder reaction [37,38,43–45]. The second method consists of incorporating a Diels–Alder structure, e.g., HODA, into the structure of a polymer chain containing PEG. Nevertheless, achieving the desired derivatizations often involves a series of distinct steps.

In the current investigation, we describe the synthesis and assessment of six urethane (meth)acrylate oligomers that incorporate inherent Diels–Alder structures within the polymer chains. These photoreactive oligomers exhibit diverse carbon chain structures, particularly varying soft segments in the form of PEGs with different molecular weights.

The resulting resins form thin polymer films cured using UV radiation. Our investigation delves into the effects of distinct molecular weights and PEG contents on the performance of the photocuring process, properties of cured coatings, and self-healing behavior. This research contributes valuable insights into the development of self-healing polymeric materials applicable to diverse industries, including coatings and the production of polymeric elements such as automobile varnishes and plastic components.

## 2. Materials and Methods

### *2.1. Materials*

All reagents used in the study were commercially available and obtained without further purification. Maleic anhydride (98%) and dibutyltin dilaurate (95%) were sourced from Alfa Aesar (Haverhill, MA, USA). Furan (≥99.9%) was purchased from Fluka (Charlotte, NC, USA). Hydroquinone (99%), polyethylene glycol PEG 600, and PEG 1000 (for synthesis) were acquired from Sigma-Aldrich (Steinheim am Albuch, Germany). Furfuryl alcohol (98%) and isophorone diisocyanate (IPDI) (98%) were supplied by Across Organics (Geel, Belgium). Polyethylene glycol PEG 400 (Pluriol E400) was provided by BASF (Ludwigshafen, Germany). 2-Hydroxypropyl acrylate (HPA) and 2-hydroxypropyl methacrylate (HPMA) were generously donated by Cognis Performance Chemicals (Hythe, UK). Analytical-grade ethanolamine and triethanolamine were sourced from Chempur (Piekary Śląskie, Poland). Diethyl ether (99.5%) and anhydrous ethanol p.a. (99.8%) were obtained from Avantor Performance Materials Poland S.A. (POCH, Gliwice, Poland). High-purity acetone, isopropanol, xylene, toluene, and dichloromethane were purchased from StanLab (Lublin, Poland).

### *2.2. Synthesis of UA-DA Prepolymers*

The synthesis of urethane acrylates with a built-in Diels–Alder structure (UA-DA) was performed according to the method outlined in [46]. 1-(hydroxymethyl)-10-oxatricyclo [5.2.1.02.6]—HODA (dec-8-ene-3,5-dione-2-aminoethanol) was produced using a modified four-step procedure [38,47–49]. Then, HODA and 10 mL dichloromethane were added to the reactor, equipped with a thermometer, magnetic stirrer, and dropper. After purging with argon gas, isophorone diisocyanate (IPDI) was applied drop by drop over one hour while stirring. Eight hours were spent stirring the reaction at 30 °C in an inert gas atmosphere. Next, PEG (400, 600, or 1000) and dibutyltin dilaurate (catalyst) were added to dichloromethane. At temperatures of 75 °C, the stirring process lasted three hours. Then, 2-hydroxypropyl acrylate (HPA) or 2-hydroxypropyl methacrylate (HPMA) and dibutyltin dilaurate were poured into the reaction mixture. The mixture was refrigerated to a temperature of 55 °C (ATR-FTIR control). The reaction continued until the -NCO group band at 2270 $cm^{-1}$ disappeared. The quantities of reagents are listed in Table 1.

**Table 1.** Amounts of substrates used for syntheses of UA-DA prepolymers.

| Sample Code | $m_{HODA}$ (g) | $m_{DD}$ (g) | $m_{IPDI}$ (g) | $M_{PEG}$ | $m_{PEG}$ (g) | $m_{DD}$ (g) | HR(M)A | $m_{HR(M)A}$ | $m_{DD}$ (g) |
|---|---|---|---|---|---|---|---|---|---|
| PEG400-HPA | 9.98 | 0.26 | 18.53 | 400 | 8.34 | 0.25 | HPA | 5.42 | 0.33 |
| PEG600-HPA | 9.35 | 0.21 | 17.45 | 600 | 11.78 | 0.21 | HPA | 5.11 | 0.30 |
| PEG1000-HPA | 9.33 | 0.31 | 17.35 | 1000 | 19.51 | 0.26 | HPA | 5.07 | 0.31 |
| PEG400-HPMA | 9.52 | 0.26 | 17.70 | 400 | 7.96 | 0.29 | HPMA | 5.73 | 0.34 |
| PEG600-HPMA | 9.47 | 0.21 | 17.59 | 600 | 11.87 | 0.22 | HPMA | 5.70 | 0.33 |
| PEG1000-HPMA | 9.23 | 0.21 | 16.92 | 1000 | 19.03 | 0.22 | HPMA | 5.49 | 0.27 |

$m_{HODA}$ represents the mass of the utilized 1-(hydroxymethyl)-10-oxatricyclo [5.2.1.02.6] dec-8-ene-3,5-dione-2-aminoethanol (HODA); $m_{DD}$ indicates the mass of the applied dibutyltin dilaurate (DD); $m_{IPDI}$ denotes the mass of the employed isophorone diisocyanate; MPEG signifies the average molecular mass of the utilized polyethylene glycol (PEG); and mPEG corresponds to the mass of the employed polyethylene glycol. HR(M)A refers to the type of (meth)acrylate employed in the synthesis, and $m_{HR(M)A}$ stands for the mass of the used (meth)acrylate.

### 2.3. General Analytical Methods for Structural Confirmation

Spectroscopic techniques, including $^{1}$H NMR, $^{13}$C NMR, and ATR-FTIR, were employed to verify the structure and purity of the synthesized compounds. The $^{1}$H nuclear magnetic resonance (NMR) spectra were obtained utilizing a BRUKER DPX-400 spectrometer (Billerica, MA, USA) operating at 400 MHz in $CD_2Cl_2$ as the solvent. Chemical shifts (ppm) were referenced to tetramethylsilane (TMS) as the internal standard. ATR-FTIR spectra were captured employing a Thermo Scientific Nicolet 380 (Waltham, MA, USA) spectrometer featuring an ATR diamond plate. The spectra were obtained in transmission mode within the range of 4000 to 400 $cm^{-1}$, with a resolution of 4 $cm^{-1}$, and analyzed using version 7.3 of the Omnic program.

### 2.4. Formulation of Coating Compositions and Cured Films

The formulation of photoreactive coating compositions involves the combination of synthesized urethane acrylate prepolymers with 3 wt.% of a radical photoinitiator, specifically ethyl(2,4,6-trimethylbenzoyl)-phenyl phosphinate (Omnirad TPOL, IGM Resins). To achieve a uniform mixture, the components were thoroughly blended in the absence of light. Subsequently, the resulting curing mixture was applied to glass substrates using a gap applicator with a thickness of 120 µm. The polymeric film was then subjected to a UV lamp (Aktiprint-mini 18-2; type: UN50029, Technigraf GmbH, Grävenwiesbach, Germany) with a UV light intensity of 200 $mW/cm^2$ at room temperature.

### 2.5. Assessment of the Photopolymerization Process and Cured Coatings Properties

The UV-curing procedure of the fabricated urethane acrylates was comprehensively characterized using Fourier transform infrared spectroscopy (FTIR) and photo-differential scanning calorimetry (photo-DSC).

FTIR analysis was conducted on a Nicolet iS5 instrument (Thermo Fisher Scientific, Waltham, MA, USA) with a scanning range of 400–4000 $cm^{-1}$ and a resolution of 4 $cm^{-1}$. Real-time IR (RT-IR)) spectroscopy facilitated in situ monitoring of the photopolymerization process by measuring the dissolution of the characteristic bonds under ultraviolet light exposure [50]. The urethane acrylates, along with an initiator mixture, were placed in a 15 mm diameter and 0.2 mm thick glass mold. Simultaneous exposure to a UV light source (mercury UV lamp, 36 W, 280–400 nm, 10 $mW/cm^2$) and an IR analyzing light beam allowed quantification of the degree of polymerization (DC) using the formula (Equation (1)):

$$DC\ (\%) = (A_0 - A_t) \cdot 100 / A_0, \quad (1)$$

where $A_0$ represents the initial peak area before irradiation, and $A_t$ denotes the peak area at time t. The photopolymerization rate ($R_p$) was determined using the below equation (Equation (2)):

$$R_p = dDC/d_t, \quad (2)$$

where t represents the irradiation time [51].

Additionally, a photo-differential scanning calorimetry (photo-DSC) instrument (Q100, TA Instruments, New Castle, DE, USA) equipped with the Omnicure S2000 UV light emitter (280–480 nm, 200 $mW/cm^2$; Excelitas Technologies, Waltham, MA, USA) was employed to isothermally monitor the UV-curing process at 25 °C in a nitrogen atmosphere for 10 min, providing insights into the photoreactivity of the synthesized systems.

The characteristics of the cured coatings were evaluated via various tests, including tack-free time, pendulum hardness test, adhesion, gloss, and yellowness index. The properties of the cured coatings were evaluated through via tests, including tack-free time, Pendulum hardness, adhesion, gloss, and yellowness index. Tack-free time, indicating the time at which the coating achieves its final technical parameters, was measured following ISO 9117. The hardness of coatings was assessed using a Persoz pendulum hardness test on a glass substrate (TQC Sheen, Capelle aan Ijssel, The Netherlands) in accordance with ISO 1522. Adhesion to glass substrates was evaluated using the cross-cut method per

PN-EN ISO 2409 (BYK, Wesel, Germany). Gloss was measured using the GLS spectrometer (SADT Development Technology Co., Ltd., Beijing, China) according to ASTM D523. The yellowness index, describing color changes, was determined using a precision colorimeter NH-145 in adherence to ASTM E313 (3NH Technology Co., Ltd., Shenzhen, China).

### *2.6. Investigation of Self-Healing Properties*

To comprehend the thermally reversible mechanism of the synthesized urethane acrylates, various methods, including DSC, TG, and FTIR, were employed. Additionally, an optical microscope was utilized to observe the self-healing properties of the cured films. This methodology was presented in detail in our previous publication [52].

The DSC method was applied to elucidate the thermally reversible mechanism of the Diels–Alder (DA) structures in the cured coatings. A DSC apparatus (Q100, TA Instruments, New Castle, DE, USA) was employed, with aluminum pans used to seal samples weighing between 7 and 10 mg. The measurements involved a heating-cooling-heating cycle in the temperature range of −90 to 300 °C, with a heating ramp of 10 °C/min.

Furthermore, the thermal stability of all obtained prepolymers was assessed via thermogravimetric (TG) analysis using the Netzsch Proteus Thermal Analysis TG 209 F1 Libra apparatus (Netzsch, Selb, Germany). Alumina crucibles were utilized, and the analysis was conducted in an oxidizing atmosphere (nitrogen flow, as protective gas; 10 $cm^3$/min and airflow—25 $cm^3$/min) over the temperature range of 25 to 1000 °C ($Al_2O_3$).

To monitor the self-healing properties of the cured films, an optical microscope was employed, allowing for a comprehensive examination of the material's ability to recover from damage.

## 3. Results and Discussion

### *3.1. Synthesis and Characterization of Urethane Acrylates*

Initially, a set of six urethane (meth)acrylate (UA-DA) featuring an embedded Diels–Alder (DA) structure was synthesized. These UA-DA oligomers exhibited variations in the chemistry of the soft segment, specifically in the molecular weight of polyethylene glycol (PEG) employed during the synthesis. The selected PEGs for extending the prepolymer chain were PEG400, PEG600, and PEG1000. Figure 1 illustrates the prepolymer chain of the obtained resins, taking into consideration the specific PEG utilized. The synthesis process involves the formation of urethane moieties via the reaction of hydroxyl groups in the HODA structure with diisocyanate (IPDI) in a molar ratio of 1:2. Subsequently, the terminal isocyanate groups react with the appropriate polyol (PEG400, PEG600, or PEG1000) and hydroxypropyl (meth)acrylate (HPA or HPMA) in an equimolar ratio.

Figure 2 illustrates the FTIR spectra of the synthesized oligomers, while the FTIR and NMR spectra obtained during the multi-step reaction can be found in the Supplementary Materials (Figures S1–S15) or detailed in our prior research [46]. The spectra exhibit characteristic bands confirming the formation of the intended structures. The confirmation of the compound's structure was based on the analysis of typical urethane peaks, including the band at approximately 3350 $cm^{-1}$ assigned to $\nu_{N–H}$, the strong bands at around 2850–3000 $cm^{-1}$ attributed to $\nu_{C–H}$, the strong bands at about 1700 $cm^{-1}$ designated as $\nu_{C=O}$, the strong bands at roughly 1520 $cm^{-1}$ assigned to $\nu_{C-N}$, and bands at approximately 1170 $cm^{-1}$ assigned to $\nu_{C-O-C}$. Additionally, vibrations specific to the Diels–Alder structure derived from the C=C bond at 3065 $cm^{-1}$ and characteristic vibrations of the double bond from acrylate at 810 $cm^{-1}$ were observed. This confirms the successful synthesis of oligomers containing Diels–Alder bonds. Any variations in the bands among different oligomers were minimal and attributed to structural differences.

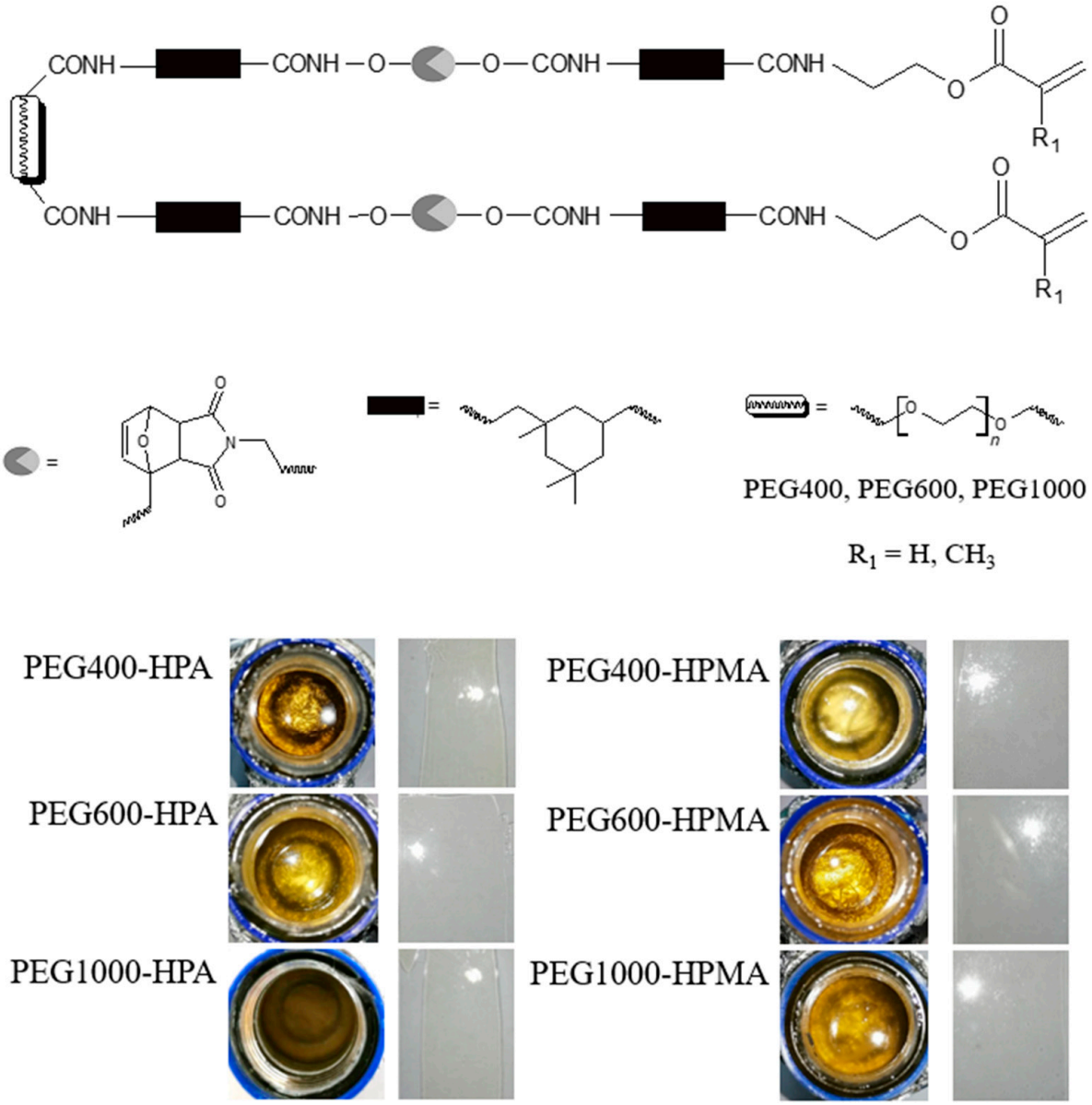


**Figure 1.** Scheme of the urethane (meth)acrylates with built-in DA structure and various soft segment molecular weights (PEG 400, PEG 600, or PEG 1000, respectively) and photoreactive groups (HPA or HPMA).

The confirmation of the chemical structure of the synthesized urethane (meth)acrylates was additionally validated via the analysis of NMR spectra. Detailed results of the $^{1}$H NMR spectra can be found in the Supplementary Materials (Figures S10–S16). Figure 3 provides a comparative illustration of the $^{1}$H NMR spectra of the obtained urethane acrylates. The analysis of the NMR spectra confirmed the identity of the synthesized compounds, and it facilitated the determination of the number "n" in the PEG chain $(OCH_2CH_2)_n$.

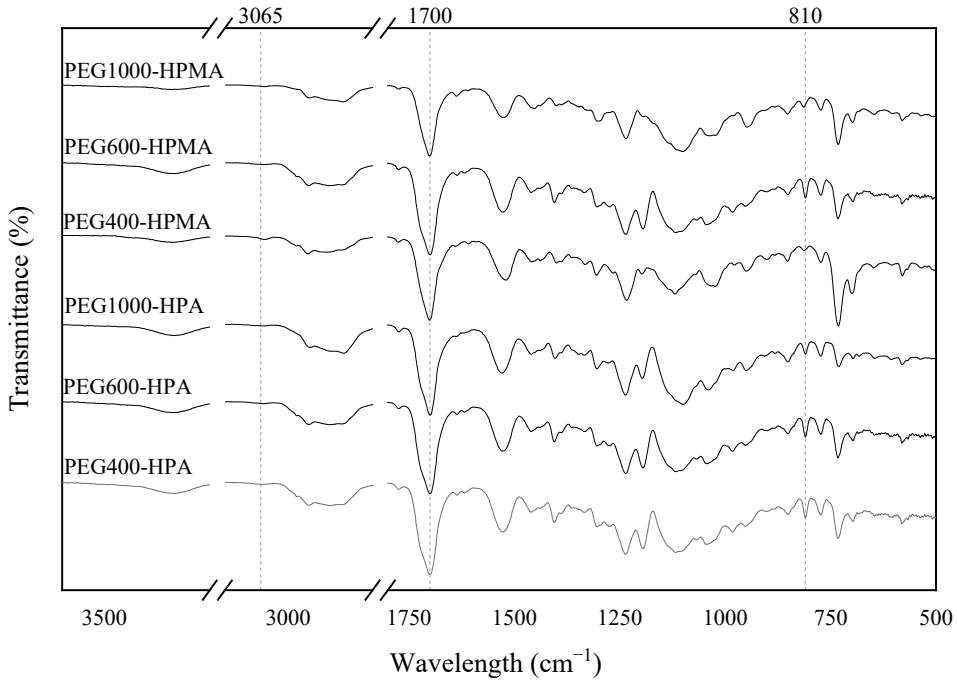


**Figure 2.** FTIR spectra of obtained urethane (meth)acrylates.

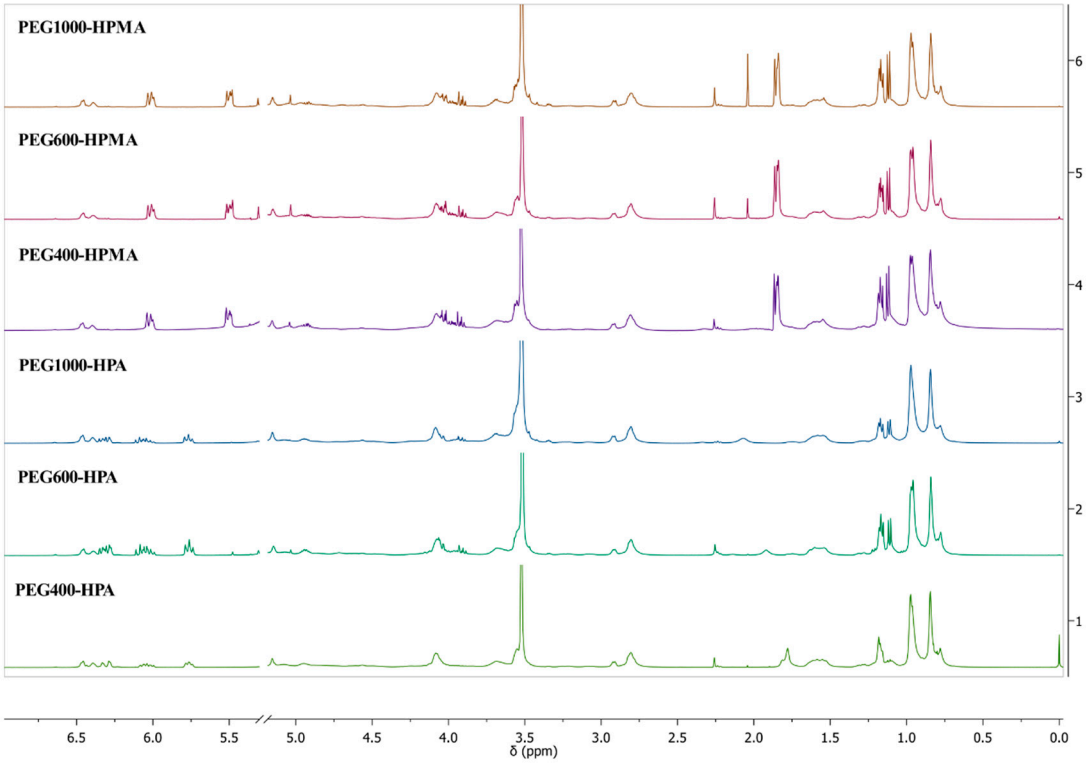


**Figure 3.** $^{1}$H NMR spectra of obtained urethane (meth)acrylates.

### *3.2. The UV Curing Process of Obtained Urethane (Meth)acrylates*

The photopolymerization process was monitored in order to determine the influence of the photocuring kinetics of the coatings on the self-healing properties. In this study, a mixture of the obtained urethane (meth)acrylate oligomers with 3 wt.% radical photoinitiator was used. The findings are depicted in Figure 4, showcasing the conversion degree of unsaturated bonds (C=C) tracked via the disappearance of the 810 cm$^{-1}$ peak and the rate

of alterations observed during UV irradiation. It is noteworthy to mention that our prior research established that photocuring did not alter the existence of the Diels–Alder (DA) structure in the prepolymer chain, a crucial factor contributing to the self-healing attributes of the coatings [46]. This paper presents the conversion degree of acrylate groups (for HPA) or methacrylate groups (for HPMA) as a result of the process initiated by UV radiation, apart from the general tendency to achieve a higher conversion of unsaturated bonds for acrylate groups compared to methacrylate groups. There are also visible dependencies of conversion changes resulting from the structure of the soft segment, i.e., the polyols used. With the increase in the length of the soft segment, a greater degree of unsaturation bonds is reacted. These significant changes are probably due to a reduction in the stiffness of the polymer network and the possibility of easier migration of radicals. The highest conversion was achieved in the case of urethane acrylate containing a soft segment in the form of polyether glycol with a molecular weight of 1000 g/mol (PEG1000-HPA; 89%) and the lowest in the case of urethane methacrylate containing a soft segment in the form of polyether glycol with a molecular weight of 400 g/mol (PEG400-HPMA; 32%). The photo-DSC method was used to determine the time to achieve maximum heat flow during photopolymerization (Table 2), which was the shortest in the case of PEG400-HPA. In addition, this oligomer also showed the highest reaction rate monitored by FTIR. Further, it was also noted that methacrylates had a higher total enthalpy of the photocuring process compared to methacrylates. The kinetic characteristics of the photopolymerization process can be used to gain a deeper knowledge of the self-healing of coatings.

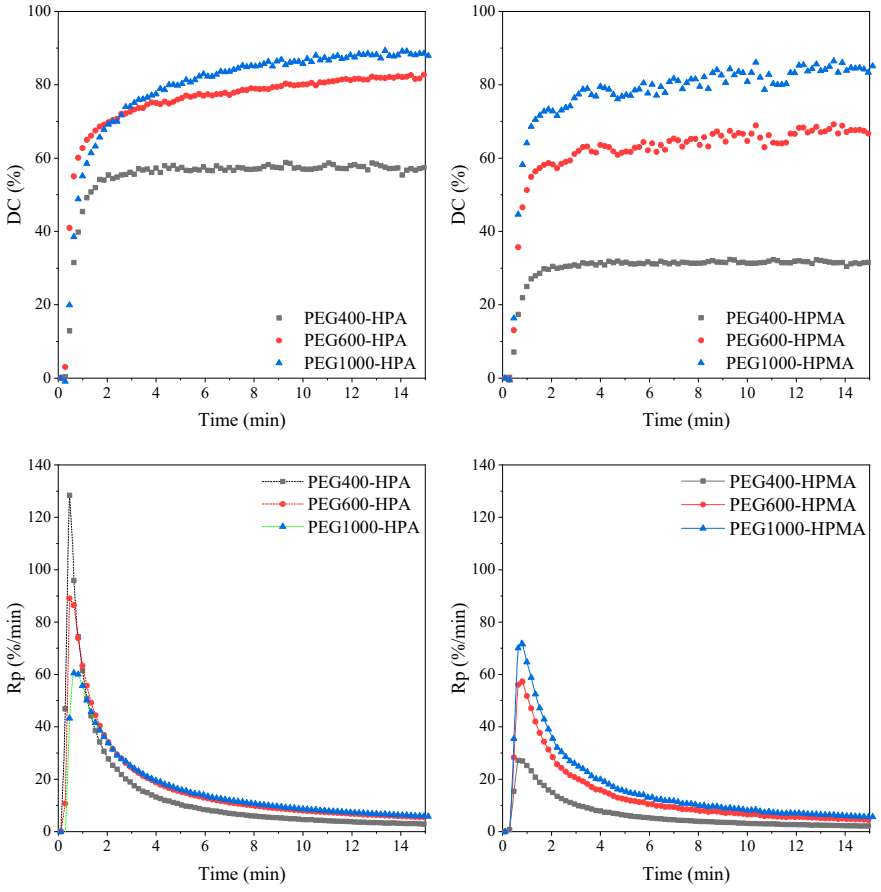


**Figure 4.** The conversion degree (DC) and photopolymerization rate (Rp) of photoreactive compositions based on urethane (meth)acrylates with built-in DA adducts (HPA—in the case of acrylate groups or HPMA—in the case of methacrylate groups) differing in the length of the soft segment of the prepolymer chain (PEG 400, 600, or 1000) which were monitored by FTIR.

**Table 2.** Characteristics of the photocuring process for UA-DA compositions, as identified via photo-DSC or FTIR methods.

| Sample Code | $\Delta H_{total}$ (J/g) | $t_{max}$ (s) | $DC_{max}$ (%) | $Rp_{max}$ (%/min) |
|---|---|---|---|---|
| PEG400-HPA | 290 | 1.8 | 57 | 128 |
| PEG600-HPA | 232 | 7.8 | 83 | 89 |
| PEG1000-HPA | 139 | 8.4 | 89 | 61 |
| PEG400-HPMA | 435 | 4.2 | 32 | 27 |
| PEG600-HPMA | 451 | 4.2 | 67 | 57 |
| PEG1000-HPMA | 465 | 4.2 | 86 | 71 |

$\Delta H_{total}$—total enthalpy of the photocuring process; $t_{max}$—time to achieve maximum heat flow (the time when there was no radiation was subtracted); $DC_{max}$—maximum conversion degree; $Rp_{max}$—the maximum rate of conversions.

### *3.3. Properties of Cured Coatings*

To investigate the impact of different soft segments in the prepolymer chain architectures of the synthesized urethane (meth)acrylates with a built-in DA structure on the cured coatings, the essential properties of the cured coatings were assessed and are detailed in Table 3. All coatings exhibited rapid surface dryness within a brief timeframe, ranging from 3 to 6 seconds. In accordance with the assumptions resulting from the characteristics of the photopolymerization process regarding the reduced stiffness of polymer networks in the case of elongation of the soft segment, harder coatings are obtained for UA containing shorter soft segments. A noticeable tendency is also to obtain harder coatings based on UA with methacrylate groups compared to UA with acrylate groups, which is probably due to the stiffer structure of the carbon chain resulting from the presence of an additional methyl group. Along with the increase in the hardness of the coatings, a slight decrease in adhesion to the substrate was observed. All coatings had excellent gloss and were colorless.

**Table 3.** Properties of the cured UA-DA coatings.

| Sample Code | Tack-Free Time (s) | Hardness | Adhesion | Gloss (GU) | Yellowness Index |
|---|---|---|---|---|---|
| PEG400-HPA | 3 | 70 | 2.5 | 146 | 5.4 |
| PEG600-HPA | 3 | 65 | 2.0 | 151 | 5.4 |
| PEG1000-HPA | 6 | 58 | 1.0 | 166 | 5.5 |
| PEG400-HPMA | 3 | 131 | 2.5 | 103 | 4.3 |
| PEG600-HPMA | 3 | 119 | 1.5 | 150 | 3.9 |
| PEG1000-HPMA | 6 | 111 | 1.5 | 151 | 3.6 |

### *3.4. Thermal Properties of Obtained Urethane (Meth)acrylates*

The thermoreversibility of the synthesized urethane (meth)acrylates was assessed for practical applications, exploring the correlation between polymer chain architecture and the self-healing performance of UV-cured coatings. Polymer behavior at elevated temperatures is known to be influenced by its structure. Therefore, these relationships were comprehensively examined using DSC, TG, and FTIR methods.

DA and retro-DA reactions were predominantly examined using differential scanning calorimetry (DSC) measurements, which entailed a heating-cooling-heating cycle for cured films of UA-DA. As depicted in Figure 5, the first heating cycles of the tested samples reveal two broad endothermic peaks corresponding to the glass transition and the rDA reaction [37,38,45,53], as anticipated. The first heating cycle of the cured samples in the given temperature-time conditions was characterized by determining (i) the glass transition temperature ($T_g$), (ii) the onset temperature of the rDA reaction ($T_{rDAonset}$), (iii) the temperature peak of the rDA reaction, and (iv) the total enthalpy of the rDA reaction ($\Delta H$). It is noted that UA-DA-based coatings with longer carbon chains in the soft segments achieve lower glass transition temperatures ($T_{gPEG1000} > T_{gPEG600} > T_{gPEG400}$), and their cured coatings have a lower hardness. Therefore, the theory explaining the generally observed trends in

the variability of $T_g$ resulting from the change in the polymer microstructure [54,55] is associated with a change in the stiffness of polymer networks and the mobility of carbon chains. The relaxation of polymer segments may also affect the self-healing ability of coatings. The clarification of the molecular correlation between Tg and polymer characteristics is valuable for the design and processing of novel synthetic materials. Furthermore, it contributes to comprehending the dynamics and managing the retention of self-healing properties. As mentioned above, the second endothermic peak is related to the retro-Diels–Alder reaction. Interestingly, the onset temperature of the rDA reaction ($T_{rDAonset}$) is lower for UA-DA with higher glass transition temperatures and starts at 91 °C for acrylates (PEG400-HPA) and 102 °C for methacrylates (PEG400-HPMA). In all the cases studied, the temperature peak of the rDA reaction is 141 ± 3 °C, respectively, in the range of 138–144 °C for acrylates and 140–141 °C for methacrylates. On the other hand, when considering the total reaction enthalpy of rDA (ΔH), a wide range of results is observed for acrylates with different lengths of the soft segment (3.46–24.58 J/g), while methacrylates show slight differences in the total reaction enthalpy of rDA (14.55–17.97 J/g). Low enthalpy may indicate a slow or difficult occurrence of the r-DA reaction, ultimately responsible for the worse self-healing properties of the coatings. In connection with the above, significant relationships are found between the microstructure of the obtained urethane (meth)acrylates and their thermal properties or ability to thermoreversibility.

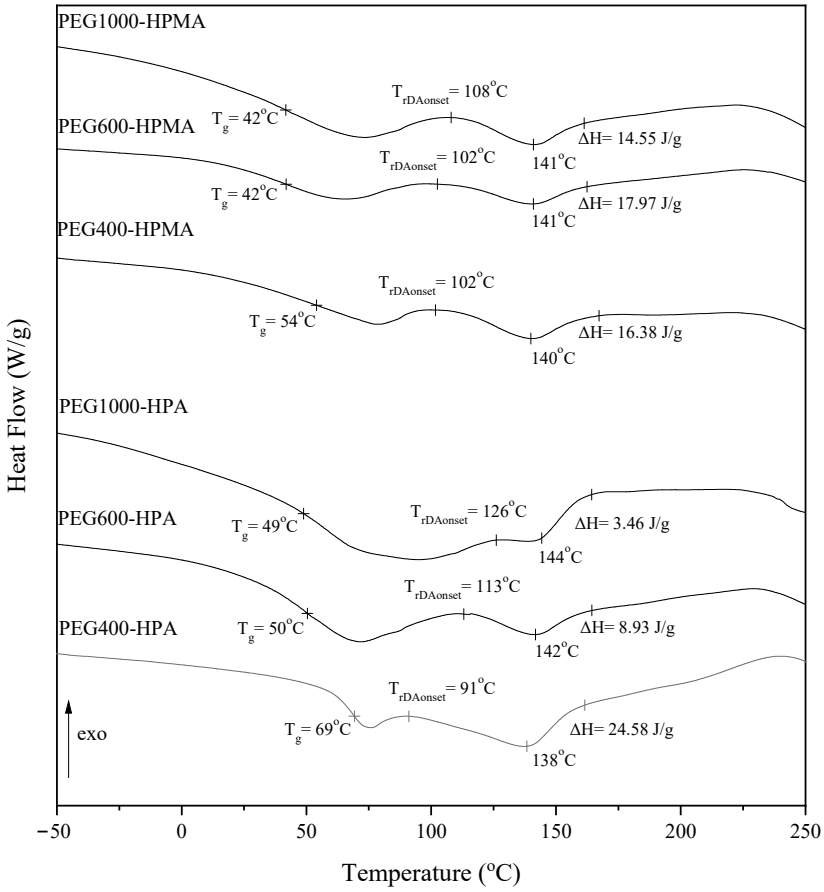


**Figure 5.** Differential scanning calorimetry (DSC) curves observed during the initial heating cycle for the UV-cured urethane (meth)acrylates with built-in DA structure and different soft segment chemistry (PEG 400, 600, or 1000).

The thermogravimetric technique was utilized to evaluate the thermal stability of the obtained oligomers, focusing on properties such as onset decomposition temperature and maximum decomposition temperature (determined from DTG curves), as summarized

in Table 4. Multi-step decomposition was observed for all analyzed urethane acrylates; however, their thermal stability was found to be at least approximately 283 °C. This testing not only affirms the robust thermal properties of the investigated oligomers, even with the presence of temperature-sensitive DA structures but also underscores the thermal stability of the self-healing properties of the obtained coatings within the tested temperature range—indicating no decomposition of the tested compounds. The TG and DTG curves of the obtained urethane (meth)acrylates are provided in the Supplementary Materials (Figures S17–S21).

**Table 4.** Thermal stability of the obtained urethane (meth)acrylates.

| Sample Code | $T_{IDT}$ (°C) | $T_{MDT}$ (°C) |
|---|---|---|
| PEG400-HPA | 291.2 | 324.0 |
| PEG600-HPA | 283.1 | 321.7 |
| PEG1000-HPA | 274.3 | 317.9 |
| PEG400-HPMA | 290.8 | 324.6 |
| PEG600-HPMA | 291.3 | 328.3 |
| PEG1000-HPMA | 307.5 | 331.9 |

$T_{IDT}$—onset decomposition temperature; $T_{MDT}$—maximum decomposition temperature.

### *3.5. Self-Healing Ability of Coatings Based on Urethane (Meth)acrylate Oligomers with Built-in DA Structure and Differences in the Length of the Soft Segment*

The evaluation of the self-healing ability of UV-cured coatings typically involves monitoring changes in scratch size on the surface. Consequently, the coatings were deliberately scratched, and alterations were observed under controlled conditions. The experiment focused on measuring the reduced crack width after subjecting the samples to elevated temperatures. Testing spanned temperatures between 70 and 120 °C, with results presented as a percentage reduction in the width of the examined cracks relative to their initial dimensions. To strike a balance between achieving successful self-healing properties of the coatings and using the lowest possible temperature, a temperature range of 70–120 °C was employed in the studies. Literature reports suggest that a temperature of 60 °C is necessary for the reconstruction of Diels–Alder (DA) bonds embedded in the chain structure of urethane acrylate (UA) oligomers. Therefore, the lower limit of the temperature used to determine the self-healing (SH) properties of cured coatings was selected at a slightly higher temperature, specifically, 70 °C. Furthermore, as the temperature of approximately 110 °C corresponds to the retro-DA (r-DA) reaction, we opted for a slightly higher temperature of 120 °C as the upper limit. Figures 6 and 7 illustrate the self-healing degree (SH,%) for all examined samples concerning changes in heating temperature, accompanied by microscopic images depicting samples with the highest degree of self-healing at specific temperatures. The degree of self-healing of all tested samples increased with the increase in the set temperature of the process and then decreased. In most cases, the increase was up to 110 °C, and in only some cases, up to 120 °C (PEG1000-HPA, PEG400-HPMA). This temperature is close to the onset temperature of the rDA reaction determined by DSC ($T_{rDAonset}$; range for acrylates: 91–126 °C; range for methacrylates: 102–108 °C). In the case of UA-DA-based coatings with acrylate groups, a general tendency to decrease the degree of self-healing with the increasing length of the soft segment was observed, especially in tests at temperatures of about 100 °C. Shorter chain oligomers with a higher degree of self-healing also had a lower rDA reaction onset temperature, a lower rDA reaction temperature peak, and a higher total enthalpy of the rDA reaction, as determined by the DSC method. A similar analogy was observed for UA-DA-based coatings with methacrylate groups. However, in this case, PEG600-HPMA reached its maximum degree of self-healing at the lowest temperature, i.e., 100 °C. In the DSC study, this sample was characterized by the highest (among methacrylates) reaction enthalpy, 17.91 J/g. The results presented contradict the anticipated outcomes based on existing literature, which suggests that longer or less complex carbon chain polymers typically yield more flexible coatings [56]. In theory,

greater mobility and facilitation of self-healing processes should be expected [57–60]. However, the observed results from the microscopic approach may be linked to the previously described examination of the Diels–Alder mechanism in UV-cured coatings conducted under varying temperature conditions.

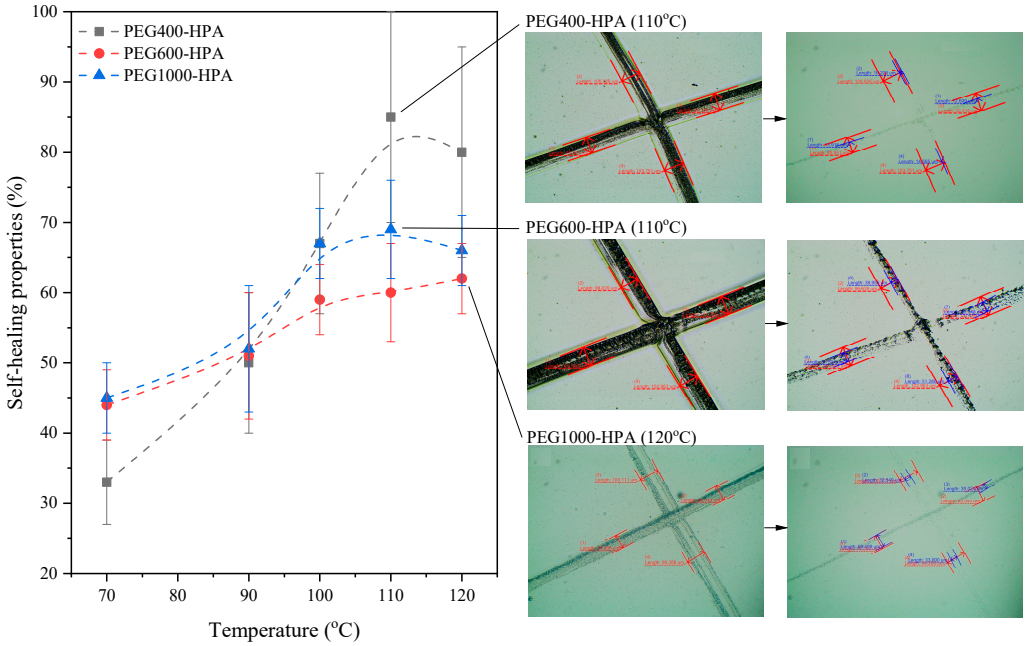


**Figure 6.** Self-healing characteristics depicted via microscopic images of urethane acrylate coatings subjected to varying temperatures.

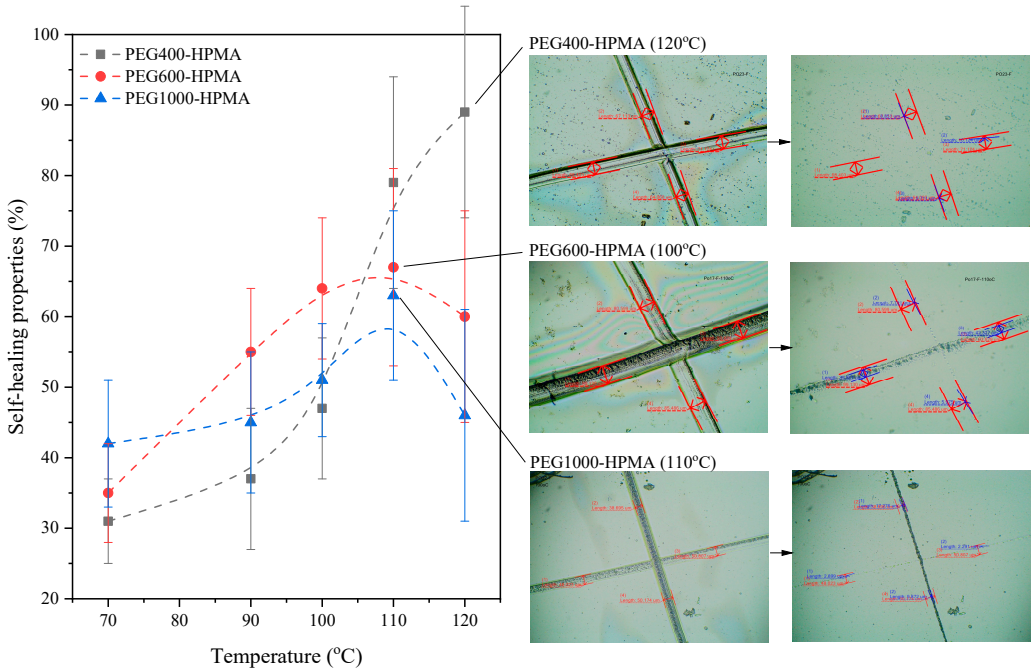


**Figure 7.** Self-healing characteristics observed in microscopic images of urethane methacrylate coatings exposed to different temperatures.

## 4. Conclusions

In summary, a series of urethane (meth)acrylate oligomers incorporating a Diels–Alder structure and distinct soft segments with varying molecular chain lengths (PEG400, PEG600, and PEG1000) were successfully synthesized. The exploration of structure–property rela-

tionships via the changes in soft segment molecular weights yielded valuable insights into the performance of these photoreactive oligomers. The investigation encompassed diverse aspects, including the kinetics of photopolymerization, cured coating properties, thermal characteristics, and self-healing capabilities. Noteworthy dependencies on C=C conversion changes during photopolymerization were observed, stemming from the specific structure of the soft segment represented by the polyols employed. The augmentation of soft segment length led to a pronounced increase in unsaturation bond reactivity, likely attributed to a reduction in polymer network stiffness and enhanced radical migration. Conversely, in the context of cured polymers, coatings derived from UA-DA with lengthier carbon chains in the soft segments exhibited lower glass transition temperatures and reduced coating hardness. This outcome was linked to alterations in polymer network stiffness and carbon chain mobility. Furthermore, the elongation of the soft segment correlated with an elevation in the onset temperature of the retro-Diels–Alder (rDA) reaction, contributing to a diminished degree of self-healing in the coatings. The elucidation of molecular relationships between C=C conversion, glass transition temperature (Tg), and polymer properties provides valuable insights for the design and processing of novel synthetic materials. Understanding these dynamics is pivotal for controlling and preserving the self-healing properties of coatings. Importantly, the strategic incorporation of Diels–Alder structures and the tailored modulation of soft segment characteristics underscore the potential of these materials in diverse applications, particularly in industries where self-healing polymeric coatings play a critical role.

**Supplementary Materials:** The following supporting information can be downloaded at https://www.mdpi.com/article/10.3390/coatings13122045/s1. Figure S1: 1H NMR HODA spectrum; Figure S2: 13C NMR HODA spectrum; Figure S3: ATR-FTIR HODA spectrum; Figure S4: Comparison of FTIR spectra investigating the reaction of receiving PEG400-HPA after 0 (blue) and 1 h (red) of reaction time. Comparison of FTIR peaks: NCO stretching at 2270 $cm^{-1}$; Figure S5: Comparison of FTIR spectra investigating the reaction of receiving PEG600-HPA after 0 (blue) and 1 h (red) of reaction time. Comparison of FTIR peaks: NCO stretching at 2270 $cm^{-1}$; Figure S6: Comparison of FTIR spectra investigating the reaction of receiving PEG1000-HPA after 0 (blue) and 1 h (red) of reaction time. Comparison of FTIR peaks: NCO stretching at 2270 $cm^{-1}$; Figure S7: Comparison of FTIR spectra investigating the reaction of receiving PEG400-HPMA after 0 (blue) and 3 h (red) reaction time. Comparison of FTIR peaks: NCO stretching at 2270 $cm^{-1}$; Figure S8: Comparison of FTIR spectra investigating the reaction of receiving PEG600-HPMA after 0 (blue) and 4 h (red) of reaction time. Comparison of FTIR peaks: NCO stretching at 2270 $cm^{-1}$; Figure S9: Comparison of FTIR spectra investigating the reaction of receiving PEG1000-HPMA after 0 (blue) and 3 h (red) of reaction time. Comparison of FTIR peaks: NCO stretching at 2270 $cm^{-1}$; Figure S10: 1H NMR spectra of PEG400-HPA; Figure S11: 1H NMR spectra of PEG600-HPA; Figure S12: 1H NMR spectra of PEG1000-HPA; Figure S13: 1H NMR spectra of PEG400-HPMA; Figure S14: 1H NMR spectra of PEG600-HPMA; Figure S15: 1H NMR spectra of PEG1000-HPMA; Figure S16: TG and DTG curves of PEG400-HPA; Figure S17: TG and DTG curves of PEG600-HPA; Figure S18: TG and DTG curves of PEG1000-HPA; Figure S19: TG and DTG curves of PEG400-HPMA; Figure S20: TG and DTG curves of PEG600-HPMA; Figure S21: TG and DTG curves of PEG1000-HPMA.

**Author Contributions:** Conceptualization, P.B.; investigation, P.B., P.O.-R., J.K. and J.R.; data curation, P.B. and P.O.-R.; writing—original draft preparation, P.B.; funding acquisition, P.B.; writing—review and editing, Y.B. and Z.C. All authors have read and agreed to the published version of the manuscript.

**Funding:** This work was supported by the National Centre for Research and Development (NCBR) (Grant No. LIDER/16/0102/L-10/18/NCBR/2019).

**Institutional Review Board Statement:** Not applicable.

**Informed Consent Statement:** Not applicable.

**Data Availability Statement:** Data are contained within the article and supplementary materials.

**Conflicts of Interest:** Author Yongping Bai was employed by the company Wuxi HIT New Material Research Institute Co., Ltd. The remaining author declare that the research was conducted in the absence of any commercial or financial relationships that could be construed as a potential conflict of interest.

## References


1. Ren, J.; Zhu, Y.; Xuan, H.; Liu, X.; Lou, Z.; Ge, L. Highly Transparent and Self-Healing Films Based on the Dynamic Schiff Base Linkage. *RSC Adv.* **2016**, *6*, 115247–115251. [CrossRef]
2. Chen, K.; Zhou, S.; Yang, S.; Wu, L. Fabrication of All-Water-Based Self-Repairing Superhydrophobic Coatings Based on UV-Responsive Microcapsules. *Adv. Funct. Mater.* **2015**, *25*, 1035–1041. [CrossRef]
3. Nawrat, C.C.; Moody, C.J. Quinones as Dienophiles in the Diels–Alder Reaction: History and Applications in Total Synthesis. *Angew. Chem. Int. Ed.* **2014**, *53*, 2056–2077. [CrossRef] [PubMed]
4. Zou, W.; Dong, J.; Luo, Y.; Zhao, Q.; Xie, T. Dynamic Covalent Polymer Networks: From Old Chemistry to Modern Day Innovations. *Adv. Mater.* **2017**, *29*, 1606100. [CrossRef] [PubMed]
5. Sahoo, R.K.; Gothwal, A.; Rani, S.; Nakhate, K.T.; Ajazuddin; Gupta, U. PEGylated Dendrimer Mediated Delivery of Bortezomib: Drug Conjugation versus Encapsulation. *Int. J. Pharm.* **2020**, *584*, 119389. [CrossRef] [PubMed]
6. Chen, X.; Sun, P.; Tian, H.; Li, X.; Wang, C.; Duan, J.; Luo, Y.; Li, S.; Chen, X.; Shao, J. Self-Healing and Stretchable Conductor Based on Embedded Liquid Metal Patterns within Imprintable Dynamic Covalent Elastomer. *J. Mater. Chem. C* **2022**, *10*, 1039–1047. [CrossRef]
7. Zheng, N.; Xu, Y.; Zhao, Q.; Xie, T. Dynamic Covalent Polymer Networks: A Molecular Platform for Designing Functions beyond Chemical Recycling and Self-Healing. *Chem. Rev.* **2021**, *121*, 1716–1745. [CrossRef]
8. Postiglione, G.; Turri, S.; Levi, M. Effect of the Plasticizer on the Self-Healing Properties of a Polymer Coating Based on the Thermoreversible Diels–Alder Reaction. *Prog. Org. Coat.* **2015**, *78*, 526–531. [CrossRef]
9. Truong, T.T.; Thai, S.H.; Nguyen, H.T.; Phung, D.T.T.; Nguyen, L.T.; Pham, H.Q.; Nguyen, L.-T.T. Tailoring the Hard–Soft Interface with Dynamic Diels–Alder Linkages in Polyurethanes: Toward Superior Mechanical Properties and Healability at Mild Temperature. *Chem. Mater.* **2019**, *31*, 2347–2357. [CrossRef]
10. Lee, T.Y.; Roper, T.M.; Jonsson, E.S.; Kudyakov, I.; Viswanathan, K.; Nason, C.; Guymon, C.A.; Hoyle, C.E. The Kinetics of Vinyl Acrylate Photopolymerization. *Polymer* **2003**, *44*, 2859–2865. [CrossRef]
11. Khudyakov, I.V. Fast Photopolymerization of Acrylate Coatings: Achievements and Problems. *Prog. Org. Coat.* **2018**, *121*, 151–159. [CrossRef]
12. Appuhamillage, G.A.; Chartrain, N.; Meenakshisundaram, V.; Feller, K.D.; Williams, C.B.; Long, T.E. 110th Anniversary: Vat Photopolymerization-Based Additive Manufacturing: Current Trends and Future Directions in Materials Design. *Ind. Eng. Chem. Res.* **2019**, *58*, 15109–15118. [CrossRef]
13. Song, W.; Li, X.; Zhao, Y.; Liu, C.; Xu, J.; Wang, H.; Zhang, T. Functional, UV-Curable Coating for the Capture of Circulating Tumor Cells. *Biomater. Sci.* **2019**, *7*, 2383–2393. [CrossRef]
14. Javadi, A.; Mehr, H.S.; Soucek, M.D. (Meth)Acrylated Poly(Ethylene Glycol)s as Precursors for Rheology Modifiers, Superplasticizers and Electrolyte Membranes: A Review: (Meth)Acrylated Poly(Ethylene Glycol) Precursors: A Review. *Polym. Int.* **2017**, *66*, 1765–1786. [CrossRef]
15. Fu, J.; Wang, L.; Yu, H.; Haroon, M.; Haq, F.; Shi, W.; Wu, B.; Wang, L. Research Progress of UV-Curable Polyurethane Acrylate-Based Hardening Coatings. *Prog. Org. Coat.* **2019**, *131*, 82–99. [CrossRef]
16. Tasic, S.; Bozic, B.; Dunjic, B. Synthesis of New Hyperbranched Urethane-Acrylates and Their Evaluation in UV-Curable Coatings. *Prog. Org. Coat.* **2004**, *51*, 320–327. [CrossRef]
17. Zhang, Q.; Huang, C.; Wang, H.; Hu, M.; Li, H.; Liu, X. UV-Curable Coating Crosslinked by a Novel Hyperbranched Polyurethane Acrylate with Excellent Mechanical Properties and Hardness. *RSC Adv.* **2016**, *6*, 107942–107950. [CrossRef]
18. Fałtynowicz, H.; Janik, H.; Kucinska-Lipka, J.; Sienkiewicz, M. Polyurethanes. In *Handbook of Thermoset Plastics*; Elsevier: Amsterdam, The Netherlands, 2022; pp. 231–262. ISBN 978-0-12-821632-3.
19. Mehravar, S.; Ballard, N.; Tomovska, R.; Asua, J.M. Polyurethane/Acrylic Hybrid Waterborne Dispersions: Synthesis, Properties and Applications. *Ind. Eng. Chem. Res.* **2019**, *58*, 20902–20922. [CrossRef]
20. Wang, Y.; Li, C.; Tuo, X.; Gong, Y.; Guo, J. Polyethylene Glycol Modified Epoxy Acrylate UV Curable 3D Printing Materials. *J. Appl. Polym. Sci.* **2021**, *138*, 50102. [CrossRef]
21. Liu, X.; Wang, Z.; Zhu, J.; Zheng, Y.; Cui, S.; Lan, M.; Li, H. Synthesis, Characterization and Performance of a Polycarboxylate Superplasticizer with Amide Structure. *Colloids Surf. A Physicochem. Eng.* **2014**, *448*, 119–129. [CrossRef]
22. Wang, Z.; Ma, Y.; Wang, Y.; Liu, Y.; Chen, K.; Wu, Z.; Yu, S.; Yuan, Y.; Liu, C. Urethane-Based Low-Temperature Curing, Highly-Customized and Multifunctional Poly(Glycerol Sebacate)-Co-Poly(Ethylene Glycol) Copolymers. *Acta Biomater.* **2018**, *71*, 279–292. [CrossRef]
23. Huang, J.; Li, A.; Li, K. Investigation of Polyurethane-Based Pressure-Sensitive Adhesives with Castor Oil as a Polyol. *Int. J. Adhes. Adhes.* **2021**, *105*, 102763. [CrossRef]

24. Zeng, L.; Song, W.; He, W.; Zhang, J.; Wang, Y.; Bian, J.; Mao, Z.; Quan, D.; Liu, J. Unconventional Passive Enhancement of Transdermal Drug Delivery: Toward a Mechanistic Understanding of Penetration Enhancers Releasing from Acrylic Pressure-Sensitive Adhesive of Patches. *Pharm. Res.* **2020**, *37*, 169. [CrossRef]
25. Xu, J.; Feng, E.; Song, J. Bioorthogonally Cross-Linked Hydrogel Network with Precisely Controlled Disintegration Time over a Broad Range. *J. Am. Chem. Soc.* **2014**, *136*, 4105–4108. [CrossRef]
26. McKinnon, D.D.; Brown, T.E.; Kyburz, K.A.; Kiyotake, E.; Anseth, K.S. Design and Characterization of a Synthetically Accessible, Photodegradable Hydrogel for User-Directed Formation of Neural Networks. *Biomacromolecules* **2014**, *15*, 2808–2816. [CrossRef]
27. Zhang, Z.; Loebus, A.; de Vicente, G.; Ren, F.; Arafeh, M.; Ouyang, Z.; Lensen, M.C. Synthesis of Poly(Ethylene Glycol)-Based Hydrogels via Amine-Michael Type Addition with Tunable Stiffness and Postgelation Chemical Functionality. *Chem. Mater.* **2014**, *26*, 3624–3630. [CrossRef]
28. Peng, F.; Liu, Y.; Li, X.; Sun, L.; Zhao, D.; Wang, Q.; Ma, G.; Su, Z. PEGylation of G-CSF in Organic Solvent Markedly Increase the Efficacy and Reactivity through Protein Unfolding, Hydrolysis Inhibition and Solvent Effect. *J. Biotech.* **2014**, *170*, 42–49. [CrossRef]
29. Xue, X.; Ji, S.; Mu, Q.; Hu, T. Heat Treatment Increases the Bioactivity of C-Terminally PEGylated Staphylokinase. *Process Biochem.* **2014**, *49*, 1092–1096. [CrossRef]
30. Pinguet, C.E.; Hoffmann, J.M.; Steinschulte, A.A.; Sybachin, A.; Rahimi, K.; Wöll, D.; Yaroslavov, A.; Richtering, W.; Plamper, F.A. Adjusting the Size of Multicompartmental Containers Made of Anionic Liposomes and Polycations by Introducing Branching and PEO Moieties. *Polymer* **2017**, *121*, 320–327. [CrossRef]
31. Nemati, H.; Roghani-Mamaqani, H.; Salami-Kalajahi, M. Preparation of Polyurethane-Acrylate and Silica Nanoparticle Hybrid Composites by a Free Radical Network Formation Method. *Bull. Mater. Sci.* **2019**, *42*, 219. [CrossRef]
32. Tungittiplakorn, W.; Kongbua, V.; Tulaphan, A.; Kaewtawee, K. Mobility of Polyethylene Glycol-Modified Urethane Acrylate (PMUA) Nanoparticles in Soils. *E3S Web Conf.* **2020**, *141*, 01002. [CrossRef]
33. Izadi, M.; Mardani, H.; Roghani-Mamaqani, H.; Salami-Kalajahi, M.; Khezri, K. Hyperbranched Poly(Amidoamine)-Grafted Graphene Oxide as a Multifunctional Curing Agent for Epoxy-Terminated Polyurethane Composites. *ChemistrySelect* **2021**, *6*, 2692–2699. [CrossRef]
34. Guan, T.; Du, Z.; Peng, J.; Zhao, D.; Sun, N.; Ren, B. Polymerizable Hydrophobically Modified Ethoxylated Urethane Acrylate Polymer: Synthesis and Viscoelastic Behavior in Aqueous Systems. *Macromolecules* **2020**, *53*, 7420–7429. [CrossRef]
35. Chen, W.; Liu, P. Pegylated Dendritic Polyurethane as Unimolecular Micelles for Tumor Chemotherapy: Effect of Molecular Architecture. *Int. J. Pharm.* **2022**, *616*, 121533. [CrossRef]
36. Xiang, H.; Wang, X.; Lin, G.; Xi, L.; Yang, Y.; Lei, D.; Dong, H.; Su, J.; Cui, Y.; Liu, X. Preparation, Characterization and Application of UV-Curable Flexible Hyperbranched Polyurethane Acrylate. *Polymers* **2017**, *9*, 552. [CrossRef]
37. Wang, Z.; Yang, H.; Fairbanks, B.D.; Liang, H.; Ke, J.; Zhu, C. Fast Self-Healing Engineered by UV-Curable Polyurethane Contained Diels-Alder Structure. *Prog. Org. Coat.* **2019**, *131*, 131–136. [CrossRef]
38. Ke, X.; Liang, H.; Xiong, L.; Huang, S.; Zhu, M. Synthesis, Curing Process and Thermal Reversible Mechanism of UV Curable Polyurethane Based on Diels-Alder Structure. *Prog. Org. Coat.* **2016**, *100*, 63–69. [CrossRef]
39. Zhengjian, Q.; Xiangxin, L.; Yueming, S.; Zhenyang, L. Synthesis, Characterization of a Novel Light Stable Cross-Linker—Isophorone Diisocyanate Terpolymer Composite. *Polym.-Plast. Technol. Eng.* **2006**, *45*, 953–956. [CrossRef]
40. Hu, S.; He, S.; Wang, Y.; Wu, Y.; Shou, T.; Yin, D.; Mu, G.; Zhao, X.; Gao, Y.; Liu, J.; et al. Self-Repairable, Recyclable and Heat-Resistant Polyurethane for High-Performance Automobile Tires. *Nano Energy* **2022**, *95*, 107012. [CrossRef]
41. Nowak, M.; Bednarczyk, P.; Mozelewska, K.; Czech, Z. Synthesis and Characterization of Urethane Acrylate Resin Based on 1,3-Propanediol for Coating Applications. *Coatings* **2022**, *12*, 1860. [CrossRef]
42. Wan, T.; Chen, D. Synthesis and Properties of Self-Healing Waterborne Polyurethanes Containing Disulfide Bonds in the Main Chain. *J. Mater. Sci.* **2017**, *52*, 197–207. [CrossRef]
43. Turkenburg, D.H.; Durant, Y.; Fischer, H.R. Bio-Based Self-Healing Coatings Based on Thermo-Reversible Diels-Alder Reaction. *Prog. Org. Coat.* **2017**, *111*, 38–46. [CrossRef]
44. Liu, J.; Zhou, Z.; Su, X.; Cao, J.; Chen, M.; Liu, R. Stiff UV-Curable Self-Healing Coating Based on Double Reversible Networks Containing Diels-Alder Cross-Linking and Hydrogen Bonds. *Prog. Org. Coat.* **2020**, *146*, 105699. [CrossRef]
45. Wang, Z.; Liang, H.; Yang, H.; Xiong, L.; Zhou, J.; Huang, S.; Zhao, C.; Zhong, J.; Fan, X. UV-Curable Self-Healing Polyurethane Coating Based on Thiol-Ene and Diels-Alder Double Click Reactions. *Prog. Org. Coat.* **2019**, *137*, 105282. [CrossRef]
46. Bednarczyk, P.; Mozelewska, K.; Klebeko, J.; Rokicka, J.; Ossowicz-Rupniewska, P. Impact of the Chemical Structure of Photoreactive Urethane (Meth)Acrylates with Various (Meth)Acrylate Groups and Built-In Diels–Alder Reaction Adducts on the UV-Curing Process and Self-Healing Properties. *Polymers* **2023**, *15*, 924. [CrossRef]
47. Lu, X.; Fei, G.; Xia, H.; Zhao, Y. Ultrasound Healable Shape Memory Dynamic Polymers. *J. Mater. Chem. A* **2014**, *2*, 16051–16060. [CrossRef]
48. Syrett, J.A.; Mantovani, G.; Barton, W.R.S.; Price, D.; Haddleton, D.M. Self-Healing Polymers Prepared via Living Radical Polymerisation. *Polym. Chem.* **2010**, *1*, 102. [CrossRef]
49. Heath, W.H.; Palmieri, F.; Adams, J.R.; Long, B.K.; Chute, J.; Holcombe, T.W.; Zieren, S.; Truitt, M.J.; White, J.L.; Willson, C.G. Degradable Cross-Linkers and Strippable Imaging Materials for Step-and-Flash Imprint Lithography. *Macromolecules* **2008**, *41*, 719–726. [CrossRef]

50. Duran, H.; Meng, S.; Kim, N.; Hu, J.; Kyu, T.; Natarajan, L.V.; Tondiglia, V.P.; Bunning, T.J. Kinetics of Photopolymerization-Induced Phase Separation and Morphology Development in Mixtures of a Nematic Liquid Crystal and Multifunctional Acrylate. *Polymer* **2008**, *49*, 534–545. [CrossRef]
51. Yin, B.; Zhang, J. A Novel Photocurable Modified Epoxy Resin for High Heat Resistance Coatings. *Colloid Polym. Sci.* **2020**, *298*, 1303–1312. [CrossRef]
52. Bednarczyk, P.; Mozelewska, K.; Nowak, M.; Klebeko, J.; Rokicka, J.; Ossowicz-Rupniewska, P. Effect of Hard Segment Chemistry and Structure on the Self-healing Properties of UV -curable Coatings Based on the Urethane Acrylates with Built-in Diels–Alder Adduct. *J. Appl. Polym. Sci.* **2023**, *140*, e54266. [CrossRef]
53. Wang, Y.; Wang, L.; Liu, H.; He, S.; Liu, X.; Liu, W.; Huang, M.; Zhu, C. Polyurethane as Smart Biocoatings: Effects of Hard Segments on Phase Structures and Properties. *Prog. Org. Coat.* **2021**, *150*, 106000. [CrossRef]
54. Dudowicz, J.; Freed, K.F.; Douglas, J.F. The Glass Transition Temperature of Polymer Melts. *J. Phys. Chem. B* **2005**, *109*, 21285–21292. [CrossRef] [PubMed]
55. Jean, Y.C. Positron Annihilation Spectroscopy for Chemical Analysis: A Novel Probe for Microstructural Analysis of Polymers. *Microchem. J.* **1990**, *42*, 72–102. [CrossRef]
56. Zafar, F.; Ghosal, A.; Sharmin, E.; Chaturvedi, R.; Nishat, N. A Review on Cleaner Production of Polymeric and Nanocomposite Coatings Based on Waterborne Polyurethane Dispersions from Seed Oils. *Prog. Org. Coat.* **2019**, *131*, 259–275. [CrossRef]
57. Zhang, E.; Shi, J.; Xiao, L.; Zhang, Q.; Lu, M.; Nan, B.; Wu, K.; Lu, M. A Highly Efficient Bionic Self-Healing Flexible Waterborne Polyurethane Elastic Film Based on a Cyclodextrin–Ferrocene Host–Guest Interaction. *Polym. Chem.* **2021**, *12*, 831–842. [CrossRef]
58. An, R.; Zhang, X.; Han, L.; Wang, X.; Zhang, Y.; Shi, L.; Ran, R. Healing, Flexible, High Thermal Sensitive Dual-Network Ionic Conductive Hydrogels for 3D Linear Temperature Sensor. *Mater. Sci. Eng. C* **2020**, *107*, 110310. [CrossRef]
59. Tong, X.; Tian, Z.; Sun, J.; Tung, V.; Kaner, R.B.; Shao, Y. Self-Healing Flexible/Stretchable Energy Storage Devices. *Mater. Today* **2021**, *44*, 78–104. [CrossRef]
60. Wu, X.; Wang, J.; Huang, J.; Yang, S. Room Temperature Readily Self-Healing Polymer via Rationally Designing Molecular Chain and Crosslinking Bond for Flexible Electrical Sensor. *J. Colloid Interface Sci.* **2020**, *559*, 152–161. [CrossRef]